HHS Public Access

Author manuscript

Liver Int. Author manuscript; available in PMC 2019 January 01.

Published in final edited form as:

Liver Int. 2018 January ; 38(1): 144–154. doi:10.1111/liv.13529.

Telomerase enzyme deficiency promotes metabolic dysfunction in murine hepatocytes upon dietary stress

Raquel M. Alves-Paiva[1,2,3], **Sachiko Kajigaya**[3], **Xingmin Feng**[3], **Jichun Chen**[3], **Marie Desierto**[3], **Susan Wong**[3], **Danielle M. Townsley**[3], **Flávia S. Donaires**[2], **Adeline Bertola**[4], **Bin Gao**[4], **Neal S. Young**[3], and **Rodrigo T. Calado**[1,2]

[1]Department of Internal Medicine, Ribeirão Preto School of Medicine, University of São Paulo, Ribeirão Preto, SP, Brazil

[2]Center for Cell-based Therapy, São Paulo Research Foundation (FAPESP), Ribeirão Preto, SP, Brazil

[3]Hematology Branch, National Heart, Lung, and Blood Institute, National Institute on Alcohol Abuse and Alcoholism, National Institutes of Health, Bethesda, MD, USA

[4]Laboratory for Liver Diseases, National Institute on Alcohol Abuse and Alcoholism, National Institutes of Health, Bethesda, MD, USA

Abstract

Background & Aims—Short telomeres and genetic telomerase defects are risk factors for some human liver diseases, ranging from non-alcoholic fatty liver disease and non-alcoholic steatohepatitis to cirrhosis. In murine models, telomere dysfunction has been shown to metabolically compromise hematopoietic cells, liver and heart via the activation of the p53-PGC axis.

Methods—*Tert*-and *Terc*-deficient mice were challenged with liquid high-fat diet. Liver metabolic contents were analysed by CE-TOFMS and liver fat content was confirmed by confocal and electronic microscopy.

Results—*Tert*-deficient but not *Terc*-deficient mice develop hepatocyte injury and frank steatosis when challenged with liquid high-fat diet. Upon high-fat diet, $Tert^{-/-}$ hepatocytes fail to engage the citric acid cycle (TCA), with an imbalance of NADPH/$NADP^+$ and NADH/NAD^+ ratios and depletion of intermediates of TCA cycle, such as cis-aconitic acid. Telomerase deficiency caused an intrinsic metabolic defect unresponsive to environmental challenge. Chemical inhibition of

Correspondence: Rodrigo T. Calado, Department of Internal Medicine, FMRP-USP – Lab. Hematologia, bloco G, subsolo – HCRP, Ribeirão Preto, SP, Brazil. rtcalado@fmrp.usp.br.

CONFLICT OF INTEREST

The authors do not have any disclosures to report.

AUTHOR CONTRIBUTIONS

Conceived and designed the experiments: RMAP SK RTC. Performed the experiments: RMAP XF JC MD SW FSD AB. Analysed the data: RMAP SK DMT RTC. Contributed reagents/materials/analysis tools: BG NSY RTC. Wrote the paper: RMAP SK RTC.

SUPPORTING INFORMATION

Additional Supporting Information may be found online in the supporting information tab for this article.

telomerase by zidovudine recapitulated the abnormal *Tert*$^{-/-}$ metabolic phenotype in *Terc*$^{-/-}$ hepatocytes.

Conclusions—Our findings indicate that in telomeropathies short telomeres are not the only molecular trigger and telomerase enzyme deficiency provokes hepatocyte metabolic dysfunction, abrogates response to environmental challenge, and causes cellular injury and steatosis, providing a mechanism for liver damage in telomere diseases.

Keywords

fatty liver; high-fat diet; metabolic dysfunction; telomerase-deficient liver

1 INTRODUCTION

Telomeres are repetitive ribonucleoprotein structures located at the termini of linear chromosomes that prevent end-to- end fusion of chromosomes, recombination and activation of the DNA damage response in cells.[1] As a result of an end-replication problem, telomeres shorten after every cell division. When critically short, they elicit cell proliferation arrest, cellular senescence and apoptosis by activation of damage pathways, including p53, p21 and PMS2.[2] In more quiescent cells, growth arrest is not critical but very short telomeres produce a degenerative metabolic status and mitochondrial dysfunction.[3]

To sustain proliferative capacity and alleviate telomere erosion, highly proliferative cells express telomerase, an enzymatic complex that elongates telomeres in the 3′ telomeric ends.[4] Telomerase is composed of the reverse transcriptase enzyme (TERT), the RNA molecule (TERC) that serves as template for its catalytic activity, and associated proteins for appropriate enzyme assembly and function.

Loss-of- function mutations in telomere-maintenance genes have been linked to accelerated telomere erosion and are aetiological in a spectrum of human diseases collectively named telomeropathies. These diseases are associated with tissue-defective -proliferative and -regenerative capacities, which ultimately can cause organ functional decline.[5–10] Mutations in *TERT* (and less frequently in *TERC*) have been described in patients with chronic liver diseases, such as non-alcoholic fatty liver disease, non-alcoholic steatohepatitis, non-cirrhotic portal hypertension and cirrhosis.[11–14] Patients with cirrhosis have been identified as having short telomeres in both hepatocytes[15] and leucocytes; [12,13] However, the mechanism(s) by which telomerase deficiency is linked to these liver disorders is not well understood. The phenotype of liver disease associated with defective telomerase, including organ fibrosis and hepatocyte steatosis, is entirely consistent with the proliferative senescence typically associated with telomere shortening. In telomeropathies, liver damage may be also a consequence of additional molecular and cellular mechanisms other than proliferation arrest.

In animal models, the telomerase-deficient mice (*Terc*$^{-/-}$) are more prone to hepatic fibrosis and inflammation after exposure to carbon tetrachloride (CCl_4). Also, forced exogenous *Terc* expression mitigates cirrhosis development.[16] It is known that p53 activation in mice with telomere dysfunction leads to mitochondrial dysfunction and metabolic failure via the

peroxisome proliferator-activated receptor gamma pathway repression.[3] However, the impact of TERT or TERC deficiency in the metabolic pathways of cells is not fully elucidated.

To address whether deficient telomerase function induces metabolic changes in hepatocytes, we investigated the hepatocytes' metabolic profile of wild type (WT) C57/BL6-J, telomerase reverse transcriptase knockout (*Tert*$^{-/-}$) and telomerase RNA component knockout (*Terc*$^{-/-}$) mice after 15 days of regular diet (RD) or liquid high-fat diet (HFD).

2 MATERIALS AND METHODS

2.1 Mice and diet

Twenty-four- to 30-week- old male WT, *Tert*$^{-/-}$ (G3) and *Terc*$^{-/-}$ (G3) mice in a C57/B6J background were used for this study. Mice were divided into two groups and fed for 15 days the following diets: (i) RD (Teklad Global 18% Protein Extruded Rodent Diet, #2018SX; Harlan), (ii) HFD (Lieber-DeCarli '82 Shake and Pour control liquid diet, #F1259SP; Bioserv), normally used as a pair-fed control. Liquid diets were administered according to Bertola et al[17] At day 16, in the morning, all mice groups were gavaged with a single dose of isocaloric dextrin maltose. The mice were always euthanized 9 hours post-gavage. *Terc*$^{-/-}$ mice were kindly provided by DePinho RA (Harvard Medical School, Boston, MA) and *Tert*$^{-/-}$ mice were purchased from the Jackson Laboratory (Bar Harbor, Maine). All animal experiments were approved by the National Heart, Lung and Blood Institute and National Institute on Alcohol Abuse and Alcoholism Animal Care and Use Committee.

2.2 Blood chemistry, hepatic lipid glycogen contents and liver histology

Blood was collected from orbital sinuses without anticoagulation to allow serum separation. Serum alanine transaminase (ALT), serum aspartate aminotransferase (AST), triglycerides, glucose and cholesterol were measured using a Clinical Chemistry Analyzer System (Vitros 250, Ortho Clinical Diagnostics, Raritan, NJ, USA). For analysis of hepatic lipid content, a total liver tissue (25–30 g) was extracted with chloroform and methanol (2:1), and triglycerides, cholesterol and glycogen contents were analysed, according to the EnzyChrom™ Assay Kit (BioAssay Systems, Hayward, CA, USA). Formalin-fixed liver samples were processed, followed by H&E staining of paraffin sections of 5-μm thickness. Glycogen and fat contents were also evaluated with PAS and Oil Red O staining respectively.

2.3 Confocal microscopy

Livers were incised into small pieces and fixed with 4% paraformaldehyde in PBS at room temperature (RT) for 1 hour. After washing with PBS, specimens were immediately stained with BODIPY493/503 (1:500 dilution; Invitrogen, Carlsbad, CA, USA) for lipid droplets in cytoplasm and with DAPI (1:500 dilution; Invitrogen) for nuclei at RT for 40 minutes. All images were acquired by Confocal Laser Scanning Microscopy with the Zeiss LSM 510 Confocal System (Confocal Zeiss MicroImaging). Fluorescence images were captured sequentially using a 360-nm or 405-nm laser line and emission of 385–470 nm for DAPI, and then a 488-nm laser line and emission between 505 and 550 nm for BODIPY. Series of

x-y-z images were collected along the z-axis at 5-to 10-μm intervals using 10× and 20× NA 0.75 objectives respectively.

2.4 Telomere measurement by qPCR and southern hybridization

DNA was extracted using the DNeasy Blood and Tissue Kit (Qiagen, Germantown, MD, USA). Mean telomere length was measured in mouse liver DNA by Southern blotting (TeloTAGGG Telomere Length Assay [Roche]) and qPCR.[10,18]

2.5 Glucose tolerance test (GTT) and insulin tolerance test (ITT)

For GTT, *Tert*$^{-/-}$ mice were injected (ip) with glucose (50% dextrose solution from Hospira through NIH Veterinary Pharmacy) at 2 mg/g body weight after 5 hours of fasting. For ITT, we injected insulin (Humulin, 100 units/mL from Lilly through NIH Veterinary Pharmacy) at 1 unit/kg body weight (ip) into mice after 2 hours of fasting. A drop of blood was obtained after piercing a pin on a tail vein for blood glucose measurement at 0, 30, 60, 90 and/or 120 minutes after glucose injection. Blood glucose was determined using a glucometer (Roche; Accu-chek).

2.6 RNA extraction and PCR array

The RNA was extracted from individual mouse livers using the RNAeasy Mini Kit (Qiagen) and subjected to complementary DNA (cDNA) synthesis using the RT^2 First Strand Kit (Qiagen). Two different RT^2 Profiler™ PCR Arrays (Fatty Liver and Wnt Signalling Pathway Assays) were employed to analyse the expression of a focused panel of genes. PCR array reaction was performed according to the manufacturer's instructions and samples were run using the 7900HT Sequence Detection System (Applied Biosystems, Foster City, CA, USA). The data analysis was performed in SDS software 2.3 (SABiosciences, Germantown, MD, USA). Genes with more than two-fold average changes were analysed using two-way hierarchical cluster analysis based on the relative expression ($2^{-\Delta\Delta Ct}$) by Ward's method (JMP version 10.0.0, SAS Institute, Arlington, VA, USA).

2.7 Analyses of metabolism

Resected liver samples were immediately frozen and stored at −80°C until metabolite extraction. Sample tissues were weighed and completely homogenized by the Multi-Beads Shocker (Yasuikikai). Homogenates were mixed with 0.5-mL chloroform and 0.2-mL ice-cold Milli-Q water. After centrifugation at 2300 *g* for 5 minutes, the supernatant was centrifugally filtrated through 5-kDa cut-off filters (Milli-pore) to remove proteins. Filtrate was centrifugally concentrated in a vacuum evaporator, dissolved with Milli-Q water and analysed by CE-TOFMS. CE-TOFMS analysis was performed by the Agilent CE System combined with a TOFMS (Agilent Technologies, Santa Clara, CA, USA), as described previously, [19] with slight modifications. Each metabolite was identified and quantified based on the peak information including *m*/*z* (mass-to- charge ratio), migration time and peak area. A total of 116 metabolites involved in glycogen synthesis, the pentose phosphate pathway, glycolysis, the TCA cycle, the urea cycle, and metabolism of polyamine, creatine, purine, glutathione, nicotinamide, choline and amino acid were quantified (Tables S2 and S3). Quantified data were evaluated for statistical significance by the Wilcoxon signed-rank test.

2.8 Statistical analysis

Data were expressed as mean ± SEM. One-way ANOVA, Mann-Whitney non-parametric test or Student's *t* test with or without Welch's correction were used when appropriate for comparison between groups, using GraphPad Prism 5.00 (GraphPad Software), and differences were considered significant if $P \leq .05$.

3 RESULTS

3.1 HFD causes liver enlargement and damage in *Tert*$^{-/-}$ mice

The WT, *Tert*$^{-/-}$ and *Terc*$^{-/-}$ mice were fed HFD or RD for 15 days (Table S1). Food intake and body weight were evaluated daily during the experimental period (Fig. S1A,B). *Tert*$^{-/-}$ mice fed HFD presented a massive accumulation of subcutaneous and abdominal fat as compared with similarly fed *Terc*$^{-/-}$ or WT mice (data not shown). Also, the livers of HFD *Tert*$^{-/-}$ mice were significantly larger and heavier than those of RD *Tert*$^{-/-}$ mice ($P < .05$) or in comparison with livers of *Terc*$^{-/-}$ and WT mice fed HFD ($P = .003$; Fig. S1C).

Serum ALT levels were elevated in HFD *Tert*$^{-/-}$ mice as compared with RD ($P = .03$), but was not significantly different in either RD or HFD *Terc*$^{-/-}$ or WT mice (Figure 1A). Likewise, HFD *Tert*$^{-/-}$ animals, but not in *Terc*$^{-/-}$ or WT mice, presented increased serum cholesterol (Figure 1C) and glucose (Figure 1D) levels in comparison with RD. In all groups, the serum AST levels increased upon HFD in comparison with RD (Figure 1B). No changes in serum triglycerides were observed among the experimental groups (Fig. S1D).

Liver triglycerides were also higher in *Tert*$^{-/-}$ ($P = .02$) and *Terc*$^{-/-}$ animals ($P = .01$) fed HFD in comparison with RD, but HFD content did not influence liver triglycerides in WT animals (Figure 1E). HFD induced significant reduction in glycogen liver content only in *Tert*$^{-/-}$ mice in comparison with RD ($P = .0002$) (Figure 1F). In *Terc*$^{-/-}$ mice, HFD also provoked an increase in cholesterol liver content ($P = .01$; Figure 1G).

Taken together, these findings demonstrate that a short course of HFD causes severe damage and abnormal metabolism only in *Tert* "knockout" hepatocytes with short telomeres. No differences in fat content, ALT, AST, cholesterol or glucose levels were found in the liver of mice null for the RNA component of telomerase *Terc* (with equally short telomeres; Fig. S2A) or in WT mice with normal telomere lengths.

3.2 High-fat diet causes liver steatosis in *Tert*$^{-/-}$ mice

Histopathological analysis of murine livers was performed after the 15-day experimental diet. Hepatic steatosis was abundant, with large lipid deposits in *Tert*$^{-/-}$ hepatocytes under HFD by H&E (Figure 1) and oil red O stainings, but not in *Terc* null or WT mice. Sixty per cent of *Tert*$^{-/-}$ mice on HFD had severe hepatic steatosis and inflammation. By confocal microscopy, fat accumulation was observed in the liver of *Tert*$^{-/-}$ animals fed HFD but not in *Terc*$^{-/-}$ or WT liver (Figure 1). Also, in all animal groups fed HFD, glycogen levels were reduced in comparison with RD (Fig. S1E). In summary, a 15-day HFD course caused lipid accumulation in *Tert*$^{-/-}$ hepatocytes with short telomeres but not in *Terc* null or WT

hepatocytes. The biochemical and histopathological findings indicate that telomerase enzyme deficiency increases hepatocyte susceptibility to dietary challenge.

3.3 Fat accumulation in *Tert*$^{-/-}$ liver is not a direct result of telomere loss alone

As only *Tert*$^{-/-}$ murine livers developed steatosis on HFD, we addressed whether this phenomenon was associated with telomere length in peripheral blood and liver from both *Tert* and *Terc* "knockout" mice. *Tert*$^{-/-}$ (G1) and *Terc*$^{-/-}$ mice had significantly shorter telomeres of peripheral blood leucocytes as compared with WT (Fig. S2A). Quantitative PCR (qPCR) and telomere restriction fragment analysis also confirmed that telomere length of *Tert*$^{-/-}$ and *Terc*$^{-/-}$ hepatocytes was equally short in comparison with WT mice (Figs S2B,C). As lipid accumulation in the liver and liver damage occurred only in *Tert* null mice, liver damage was not strictly associated with telomere erosion, but appeared to be a consequence of *Tert* enzyme deficiency.

3.4 Glucose metabolism was not altered by HFD in Tert null mice

As liver fat accumulation suggested impaired lipid metabolism, and as fat accumulates in metabolic syndrome and diabetes, we tested whether *Tert*$^{-/-}$ mice exhibited abnormal glucose metabolism using the GTT. *Tert*$^{-/-}$ mice tended to have higher plasma glucose levels after dextrose injection in comparison with WT, suggesting lower glucose tolerance, but these differences were not statistically significant (Figure 2A). *Tert*$^{-/-}$ and WT mice also appeared to be equally sensitive to insulin injection by the insulin tolerance test (ITT), as measured by plasma glucose levels (Figure 2B). These results suggested that glucose metabolism was not significantly altered by HFD in *Tert* null mice.

3.5 Chemical inhibition of Tert induces liver steatosis in *Terc*$^{-/-}$ mice

To test whether liver injury was caused by Tert enzyme deficiency, telomerase was chemically inhibited with zidovidine (AZT; 400 mg/kg/d—ip) in *Terc*$^{-/-}$ and WT mice during HFD intake. Telomerase inactivation led to an increased fat accumulation in *Terc*$^{-/-}$ livers, but not in WT murine hepatocytes. Although no significant differences were found in ALT, AST, cholesterol or glucose serum levels (Figure 3A–D), serum and liver triglycerides levels were increased in *Terc*$^{-/-}$ mice treated with AZT and HFD, but not in WT mice under similar conditions ($P = .01$; Figure 3E; Fig. S3A). Liver cholesterol was reduced in both WT and *Terc*$^{-/-}$ mice after HFD and AZT treatment, without significant alteration detected in liver glycogen content (Figure 3F,G).

Hepatic steatosis was evident in *Terc*$^{-/-}$ livers treated with AZT after HFD, as shown by H&E (Figure 3H) and oil red O staining (Figure 3H). Confocal microscopy showed fat accumulation in *Terc*$^{-/-}$ livers, but not in WT livers (Figure 3H). The glycogen content in both WT and *Terc*$^{-/-}$ livers appeared to be increased (Fig. S3B). These findings indicate that Tert chemical inhibition recapitulates in *Terc*$^{-/-}$ mice the phenotype observed in *Tert*$^{-/-}$ animals caused by HFD. These results indicate that HFD-induced liver damage is mediated by telomerase enzymatic function abrogation and short telomeres.

3.6 HFD represses fatty liver-target genes in *Tert*$^{-/-}$ and *Terc*$^{-/-}$ livers

We also investigated the expression of genes related to lipid metabolism in WT, *Tert*$^{-/-}$ *and* *Terc*$^{-/-}$ livers. In HFD *Tert*$^{-/-}$ and *Terc*$^{-/-}$ animals, the genes related to glucose uptake, including the *Gck* (glucokinase), *Gsk3*-β (glycogen synthase kinase 3 activity), *Pklr* (pyruvate kinase) *and Rxra* (a transcriptional regulator) ($P < .05$) (Figure 4A–D), and lipid uptake, such as *Cpt1* (carnitine palmitoyltransferase 1) and *Acaca* (Acetyl-CoA carboxylase) were upregulated (Figure 4C,D). Reduced expression of *Fabp5* (Fatty acid-binding protein 5), which plays an important role in systemic regulation of lipid and glucose metabolism,[17] was detected in *Tert*$^{-/-}$ ($P = .04$) but not in *Terc*$^{-/-}$ livers (Figure 4C,D). Additionally, mitochondrial biogenesis-related genes were downregulated in both HFD *Tert*$^{-/-}$ and *Terc*$^{-/-}$ livers (Figure 4C–E).

In HFD *Tert*$^{-/-}$ (G1) livers, the PPAR-target genes were upregulated (Fig. S4A), along with the *Acaca*, *Pklr*, *Cpt1* and *Fasn* (fatty acid synthase) genes (Fig. S4C,D). However, no statistical differences were found in the expression of genes involved in carbohydrate metabolism (Fig. S4B). HFD reduced the expression of *Fabp5* ($P = .04$) in *Tert*$^{-/-}$ (G1) livers, as observed in *Tert*$^{-/-}$ (G3) livers (Figure 4A).

By comparing *Tert*$^{-/-}$ and *Terc*$^{-/-}$ livers under RD conditions, genes involved in insulin signalling and cholesterol metabolism, including *Insr* (insulin receptor) and *Abca1* (ATP-binding cassette), respectively, were upregulated in *Tert*$^{-/-}$ in comparison with *Terc*$^{-/-}$ livers (Figure 4F,G). Therefore, different dietary conditions did not modulate the gene expression in WT livers.

3.7 HFD causes liver abnormal metabolism in *Tert*$^{-/-}$ mice

In order to evaluate the potential metabolic changes involved in liver damage in *Tert* null mice after HFD, we assessed a total of 116 metabolites by the targeted quantitative analysis of the liver metabolome. Principal component (PC) analysis was conducted to compare overall metabolomics profiles in murine livers. Under RD, *Tert*$^{-/-}$ and *Terc*$^{-/-}$ liver metabolomes clustered together and were significantly different from WT livers (PC1; Figure 5A). In response to 15 days of HFD, both WT and *Terc*$^{-/-}$ livers showed significant metabolic changes (PC2). However, *Tert*$^{-/-}$ livers did not show any significant metabolome changes after HFD, which suggests a broad metabolic dysfunction in these animals.

A detailed analysis showed that under RD, the glycogen synthesis was impaired in *Tert*$^{-/-}$ and *Terc*$^{-/-}$ animals in comparison with WT livers (Figure 5B–D). Upon HFD, *Terc*$^{-/-}$ and WT livers showed reduction in glycogen synthesis, whereas *Tert*$^{-/-}$ livers were minimally affected (Figure 5B–D). These findings suggest that the diet challenge was unable to modulate glycogen metabolism in *Tert*-deficient animals.

The pentose phosphate pathway analysis revealed that $NADP^+$ and NADPH balance was deregulated in both *Tert*$^{-/-}$ and *Terc*$^{-/-}$ livers under RD. While $NADP^+$ levels were comparable among the three groups under RD, NADPH levels were significantly lower in both *Tert*$^{-/-}$ and *Terc*$^{-/-}$ as compared with WT livers, resulting in decreased NADPH/$NADP^+$ ratios (Figure 5E–G). After HFD, however, WT and *Terc*$^{-/-}$ hepatocytes showed significant reduction in $NADP^+$ levels but only *Terc*$^{-/-}$ mice were able to restore the

NADPH/NADP$^+$ ratio to normal (Figure 5E–G), indicating that *Tert*$^{-/-}$ hepatocytes fail to inhibit the pentose phosphate pathway upon HFD.

The glycolysis pathway was also impaired in *Tert*$^{-/-}$ and *Terc*$^{-/-}$ livers under RD, as shown by reduced lactate/pyruvate ratios (Figure 5H). In *Terc*$^{-/-}$ livers, lactate/pyruvate ratios were at near normal after HFD. However, glycolysis was repressed in *Tert*$^{-/-}$ livers after HFD, as the lactate/pyruvate ratio remained unchanged (Figure 5H). Higher pyruvate levels were noticed in *Tert*$^{-/-}$ and *Terc*$^{-/-}$ livers under RD as compared with WT (Figure 5H) and increased pyruvate associated with a reduction in lactate (Figure 5J). However, both WT and *Terc*$^{-/-}$ livers significantly reduced pyruvate upon HFD, whereas *Tert*$^{-/-}$ livers showed an increased pyruvate concentration (Figure 5I). NAD$^+$ was slightly decreased in *Tert*$^{-/-}$ and *Terc*$^{-/-}$ livers fed RD in comparison with WT, resulting in reduced NADH/NAD$^+$ ratios (Figure 5K,L). After HFD, WT and *Terc*$^{-/-}$ livers consumed NAD$^+$, significantly reducing its concentration and increasing NADH/NAD$^+$ ratios, whereas *Tert*$^{-/-}$ livers maintained increased NAD$^+$ levels and even lower NADH/NAD$^+$ ratio (Figure 5K,L).

We also observed abnormalities in the TCA cycle (Figure 5M–P). Aconitate, an intermediate in the TCA cycle, was completely depleted in *Tert*$^{-/-}$ and *Terc*$^{-/-}$ livers (Figure 5P). After HFD, WT and *Terc*$^{-/-}$ livers showed reduction in acetyl-CoA concentrations maintaining malate and fumarate levels, whereas in *Tert*$^{-/-}$ livers, malate and fumarate were severely depleted (Figure 5M–O), and aconitate remained undetectable.

Depletion of intermediates would be predicted to block completion of the TCA cycle and we hypothesized that amino acid catabolism provided the necessary intermediates.[20] Under RD, liver aspartate, serine, lysine and glycine levels were comparable among the three groups (Figure 5Q–T). After HFD, WT and *Terc*−/− livers appeared to maintain the TCA cycle via amino acid metabolism, but *Tert*−/− livers contained reduced amounts of glucogenic amino acids (Figure 5Q–T).

4 DISCUSSION

In our study, the hepatocytes of mice null for *Tert* or *Terc* genes and with short telomeres presented abnormal metabolome profiles in comparison with WT. When challenged for a short period with fatty diet, *Tert*$^{-/-}$ livers but not *Terc*$^{-/-}$ were unable to modulate genes involved in specific metabolic pathways, resulting in clinical liver steatosis, severe hepatocyte injury and broad metabolic dysfunction. Liver damage was recapitulated when *Terc* null animals were fed HFD and telomerase was inhibited by zidovudine.

Dysfunctional telomeres diminish mitochondrial mass and energy production in heart and liver by activating p53, which, in turn, represses peroxisome proliferator-activated receptor gamma, coactivator 1 alpha and beta (*PGC-1*α and *PGC-1*β).[3] Here, we identified an additional mechanism for metabolic failure in telomerase-deficient mice. Metabolic defects were evident in *Tert*$^{-/-}$ murine livers only when challenged with dietary stress. However, *Tert* deficiency did not appear to exert its metabolic effects by repressing *Ppar*α. Our data support an indirect mechanism via the downregulation of genes (*CD36*, *Fabp5*) that negatively regulate the *Ppar*α signalling pathway. Although mitochondria in WT and *Tert*$^{-/-}$

murine livers appeared morphologically normal by electron microscopy, they were functionally impaired in *Tert*$^{-/-}$ livers, as inferred from the disruption of the TCA cycle (Table S4; Fig. S5).

In marked contrast to WT and *Terc*$^{-/-}$ livers, *Tert*$^{-/-}$ livers did not mount an appropriate metabolic response to high fat intake, compatible with metabolic failure. This behaviour was replicated with chemical inhibition of telomerase in *Terc*$^{-/-}$ animals. However, it is not clear how telomerase deficiency promotes this phenotype. Telomerase has multiple functions other than telomere elongation[21] and recruits hair follicle stem cells from resting to proliferation in the absence of Terc,[22] by a mechanism mediated by the Myc and Wnt pathways.[23] However, we did not detect changes in Wnt pathway components in *Tert*-deficient livers (data not shown). We speculate that telomerase may modulate gene transcription and interfere with cell metabolism, as telomere-associated factors interact with extra-telomeric regions of the genome to regulate gene expression.[24]

Clinical studies have recently addressed the efficacy of Imetelstat, a telomerase inhibitor, in the treatment of myeloproliferative disorders. [25,26] However, in both studies, abnormal increases in liver function tests (bilirubin, AST, ALT) were very frequent, suggesting that the liver is susceptible to damage upon telomerase chemical inhibition without measurable changes in telomere length. Indeed, liver disease is a common feature of telomeropathy patients. In agreement with our current findings, we have previously observed that individuals carrying *TERT* mutations are more prone to liver injury (cirrhosis, steatosis and nodular regenerative hyperplasia) than are patients with *TERC* mutations.[11–13]

Our findings suggest that Tert deficiency provokes hepatocyte metabolic dysfunction and cellular injury resulting in fat accumulation in the liver, and impairment of mitochondrial function (Fig. S6). These observations provide an additional molecular mechanism for liver pathology in telomeropathies. Longer exposure of telomerase-deficient mice to HFD may help clarify how hepatic disease develops in telomeropathies and to screen molecules to prevent liver damage in the setting of telomerase deficiency.

Supplementary Material

Refer to Web version on PubMed Central for supplementary material.

Acknowledgments

The authors thank Drs. M.C. Foss-Freitas, L. N. Zambelli Ramalho and L. Alberici for insightful discussions and Ms. S. N. Bresciani for art support.

Funding information

This work was supported by São Paulo Research Foundation (FAPESP) grant 13/08135-2 (R.M.A.-P., F.S.D., R.T.C.) and Divisions of Intramural Research of the NHLBI (S.K., J.C., M.D., S.W., D.M.T., N.S.Y.) and the NIAAA (A.B., B.G.). R. M. Alves-Paiva's postdoctoral scholarship was supported by FAPESP (grants 11/18313-0 and 12/00449-5). Handling Editor: Isabelle Leclercq

Abbreviations

ALT alanine transaminase

AST	aspartate aminotransferase
AZT	zidovudine/azidothymidine
GTT	glucose tolerance test
HFD	high-fat diet
ITT	insulin tolerance test
NAFLD	non-alcoholic fatty liver disease
NASH	non-alcoholic steatohepatitis
RD	regular diet
Terc	RNA component of telomerase
Tert	telomerase reverse transcriptase

References

1. Blackburn EH. Switching and signaling at the telomere. Cell. 2001; 106:661–673. [PubMed: 11572773]
2. Blasco MA. Telomere length, stem cells and aging. Nat Chem Biol. 2007; 3:640–649. [PubMed: 17876321]
3. Sahin E, Colla S, Liesa M, et al. Telomere dysfunction induces metabolic and mitochondrial compromise. Nature. 2011; 470:359–365. [PubMed: 21307849]
4. Greider CW, Blackburn EH. A telomeric sequence in the RNA of Tetrahymena telomerase required for telomere repeat synthesis. Nature. 1989; 337:331–337. [PubMed: 2463488]
5. Cohen SB, Graham ME, Lovrecz GO, et al. Protein composition of catalytically active human telomerase from immortal cells. Science. 2007; 315:1850–1853. [PubMed: 17395830]
6. Sauerwald A, Sandin S, Cristofari G, et al. Structure of active dimeric human telomerase. Nat Struct Mol Biol. 2013; 20:454–460. [PubMed: 23474713]
7. Calado RT, Young NS. Telomere diseases. N Engl J Med. 2009; 361:2353–2365. [PubMed: 20007561]
8. Townsley DM, Dumitriu B, Young NS. Bone marrow failure and the telomeropathies. Blood. 2014; 124:2775–2783. [PubMed: 25237198]
9. Yamaguchi H, Calado RT, Kajigaya S, et al. Mutations in *TERT*, the gene for telomerase reverse transcriptase, in aplastic anemia. N Engl J Med. 2005; 352:1413–1424. [PubMed: 15814878]
10. Winkler T, Hong SG, Decker JE, et al. Defective telomere elongation and hematopoiesis from telomerase-mutant aplastic anemia iPSCs. J Clin Invest. 2013; 123:1952–1963. [PubMed: 23585473]
11. Calado RT, Regal JA, Kleiner DE, et al. A spectrum of severe familial liver disorders associate with telomerase mutations. PLoS One. 2009; 4:e7926. [PubMed: 19936245]
12. Calado RT, Brudno J, Mehta P, et al. Constitutional telomerase mutations are genetic risk factors for cirrhosis. Hepatology. 2011; 53:1600–1607. [PubMed: 21520173]
13. Hartmann D, Srivastava U, Thaler M, et al. Telomerase gene mutations are associated with cirrhosis formation. Hepatology. 2011; 53:1608–1617. [PubMed: 21520174]
14. Diehl AM, Chute J. Underlying potential: cellular and molecular determinants of adult liver repair. J Clin Invest. 2013; 123:1858–1860. [PubMed: 23635782]
15. Wiemann SU, Satyanarayana A, Tsahuridu M, et al. Hepatocyte telomere shortening and senescence are general markers of human liver cirrhosis. FASEB J. 2002; 16:935–942. [PubMed: 12087054]

16. Rudolph KL, Chang S, Millard M, Schreiber-agus N, DePinho RA. Inhibition of experimental liver cirrhosis in mice by telomerase gene delivery. Science. 2000; 287:1253–1258. [PubMed: 10678830]
17. Bertola A, Mathews S, Ki SH, Wang H, Gao B. Mouse model of chronic and binge ethanol feeding (the NIAAA model). Nat Protoc. 2013; 8:627–637. [PubMed: 23449255]
18. Gutierrez-Rodrigues F, Santana-Lemos BA, Scheucher PS, Alves-Paiva RM, Calado RT. Direct comparison of flow-FISH and qPCR as diagnostic tests for telomere length measurement in humans. PLoS One. 2014; 9:e113747. [PubMed: 25409313]
19. Ohashi Y, Hirayama A, Ishikawa T. Depiction of metabolome changes in histidine-starved *Escherichia coli* by CE-TOFMS. Mol Biosyst. 2008; 4:135–147. [PubMed: 18213407]
20. Nelson, DL., Cox, MM. Lehninger Principles of Biochemistry. Gordonsville, VA: W. H. Freeman; 2004. p. 601-630.
21. Calado RT, Chen J. Telomerase: not just for the elongation of telomeres. BioEssays. 2006; 28:109–112. [PubMed: 16435298]
22. Sarin KY, Cheung P, Gilison D, et al. Conditional telomerase induction causes proliferation of hair follicle stem cells. Nature. 2005; 18:1048–1052.
23. Choi J, Southeworth L, Sarin KY, et al. *TERT* promotes epithelial proliferation through transcriptional control of a Myc-and Wnt-related developmental program. PLoS Genet. 2008; 4:e10. [PubMed: 18208333]
24. Ye J, Renault VM, Jamet K, Gilson E. Transcriptional outcome of telomere signalling. Nat Rev Genet. 2014; 15:491–503. [PubMed: 24913665]
25. Baerlocher GM, Leibundgut EO, Ottmann OG, et al. Telomerase inhibitor imetelstat in patients with essential thrombocythemia. N Engl J Med. 2015; 373:920–928. [PubMed: 26332546]
26. Tefferi A, Lasho TL, Begna KH, et al. A pilot study of the telomerase inhibitor imetelstat for myelofibrosis. N Engl J Med. 2015; 373:908–919. [PubMed: 26332545]

Key points

- Hepatocytes deficient for the telomerase reverse transcriptase display abnormal metabolic profile
- *Tert*$^{-/-}$ hepatocytes fail to engage genes involved in the metabolic response to fatty diet and the tricarboxylic acid (TCA) cycle is severely repressed
- TERT depletion may impair mitochondrial function, provoking hepatocyte metabolic dysfunction resulting in fat accumulation in the liver.
- Telomerase enzyme deficiency combined with short telomeres cause metabolic abnormalities in hepatocytes.

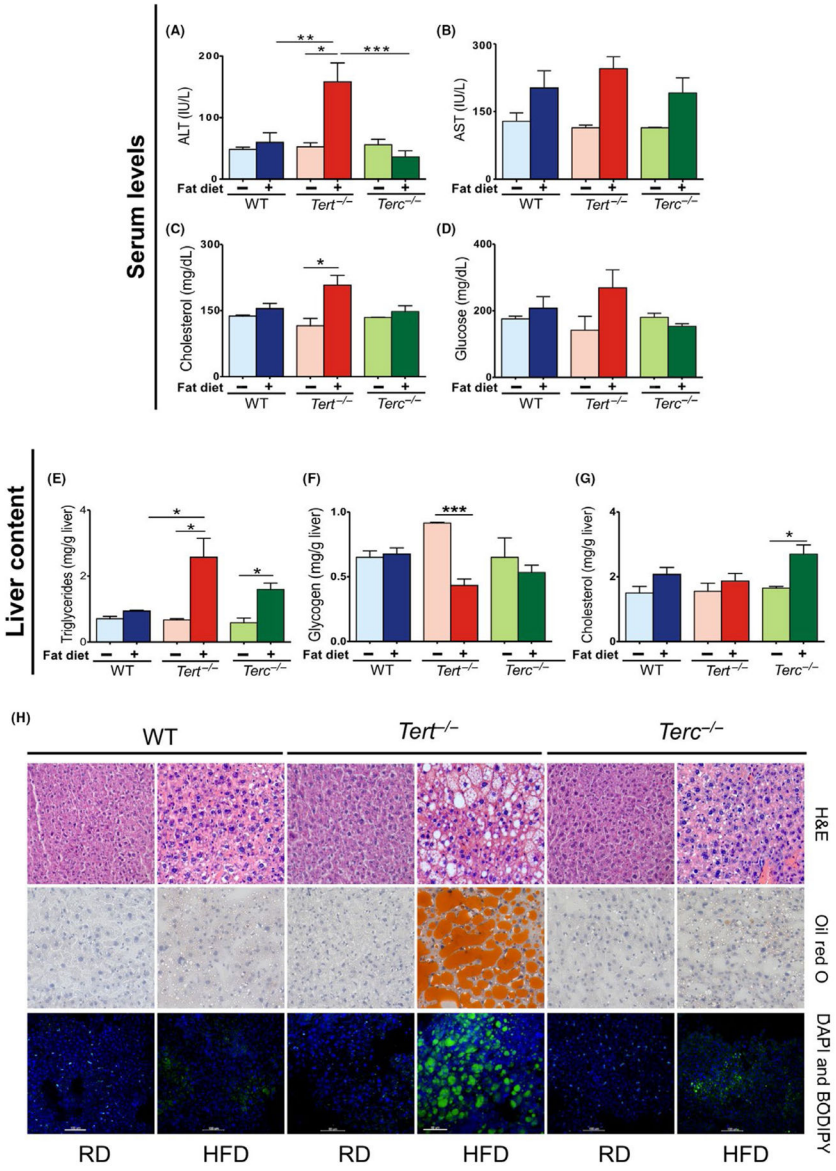

FIGURE 1.

Effects of 15-d HFD in *Tert*$^{-/-}$, *Terc*$^{-/-}$ and WT male mice. Murine serum levels were quantified under RD and HFD conditions: (A) ALT (IU/L), (B) AST(IU/L), (C) cholesterol (mg/dL), (D) glucose (mg/dL) and murine liver content (mg/g of liver) were quantified under RD and HFD conditions: (E) triglycerides, (F) glycogen and (G) cholesterol. (H) Representative microscopy images of WT, *Tert*$^{-/-}$ and *Terc*$^{-/-}$ mouse liver sections: H&E or oil red O staining (light microscopy); and DAPI and BODIPY staining (confocal microscopy). Error bars indicate mean ±SEM. **P* < .05 for the samples compared with RD conditions by Student's one-tailed *t* test. Data represent WT (RD, n = 2; HFD, n = 7), *Tert*$^{-/-}$ (RD, n = 3; HFD, n = 4) and *Terc*$^{-/-}$ (RD, n = 2; HFD, n = 6) from two independent experiments. ***P* = .0026; ****P* < .001

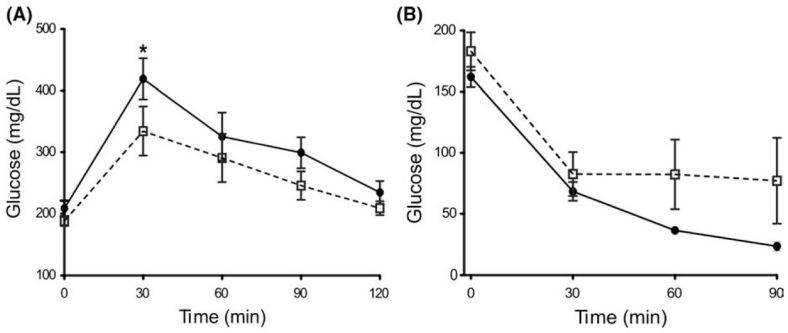

FIGURE 2.

Glucose clearance in *Tert*$^{-/-}$ and WT mice. (A) Blood glucose measurement at time 0–120 min after 50% Dextrose ip injection. (−) or (−) corresponds to *Tert*$^{-/-}$ (n = 8) or WT (n = 9) mice respectively (also applies to panels b). *$P < .05$ at time point 30 min. (B) Blood glucose measurement at time 0–90 min after insulin (Humulin) injection (ip). No influence detected in glucose clearance in *Tert*$^{-/-}$ (n = 4) or WT (n = 7) mice. Error bars indicate mean ±SEM. *$P < .05$ for the samples compared with WT conditions by Student's one-tailed *t* test

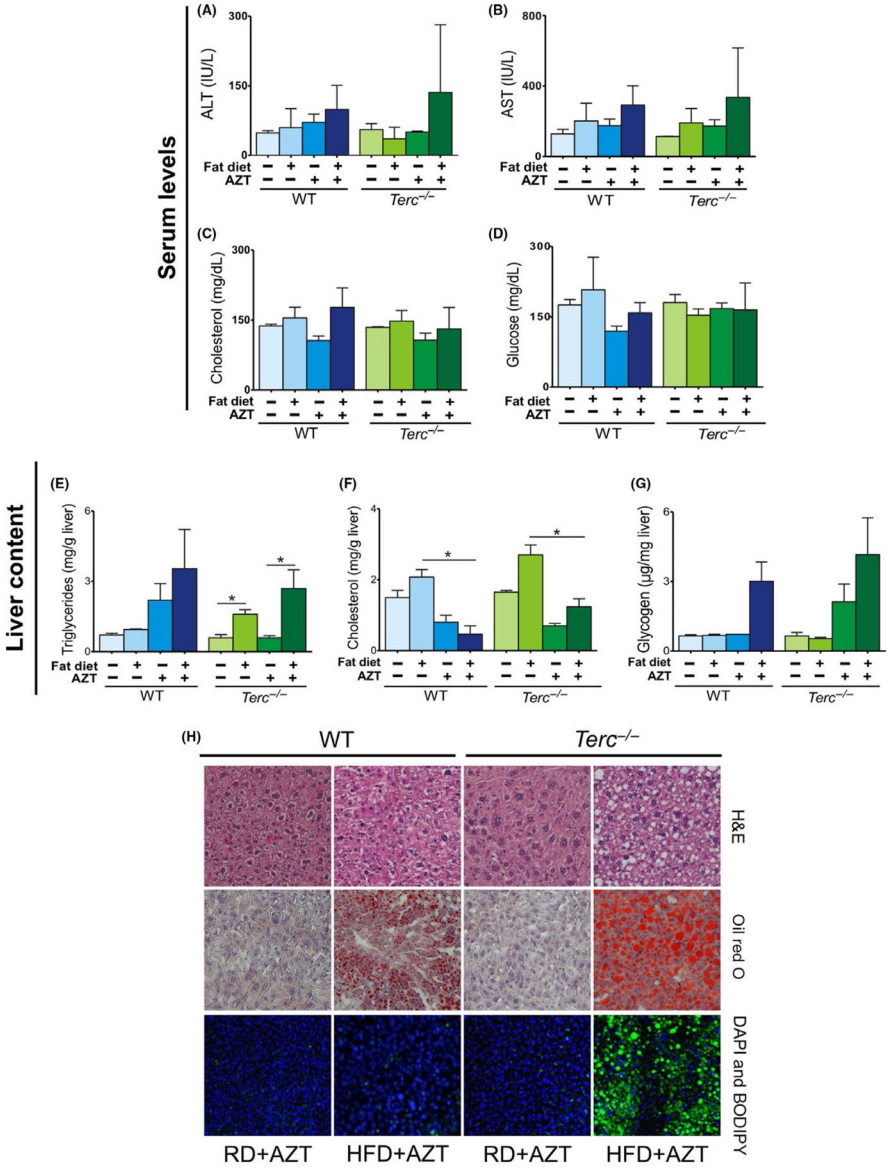

FIGURE 3.

Effects of 15-d HFD and AZT treatment in WT and *Terc*$^{-/-}$ male mice. Murine serum levels were quantified under RD and HFD conditions: (A) ALT (IU/L), (B) AST (IU/L), (C) cholesterol (mg/dL) and (D) glucose (mg/dL). Murine liver content (mg/g of liver) were quantified under RD and HFD conditions: (E) triglycerides, (F) cholesterol and (G) glycogen. (H) Representative microscopy images of WT and *Terc*$^{-/-}$ mouse liver sections: H&E or oil red O staining (light microscopy); and DAPI and BODIPY staining (confocal microscopy). Error bars indicate mean ±SEM. **P* < .05 for the samples compared with RD conditions by Student's one-tailed *t* test. Data represent WT (RD, n = 2; HFD, n = 7; RD + AZT, n = 2; HFD + AZT, n = 7) and *Terc*$^{-/-}$ (RD, n = 2; HFD, n = 6; RD + AZT, n = 2; HFD + AZT, n = 5) from two independent experiments

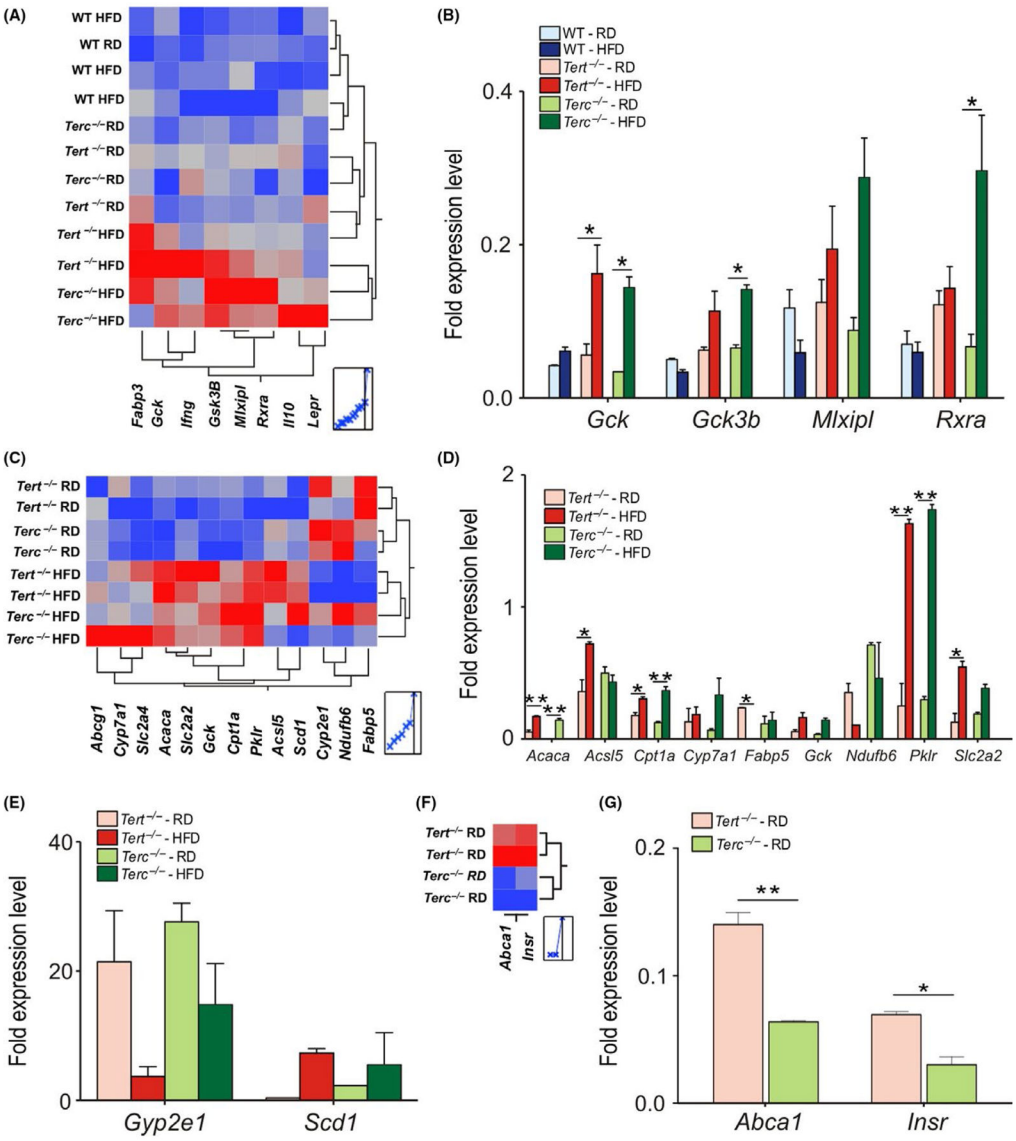

FIGURE 4.

Gene expression profiles in the liver of 6-month- old male mice fed RD and HFD for 15 d. (A) Heat map of hepatic expression of fatty liver genes affected by HFD exposure. Relative levels of gene expression are colour coded: the red or the blue colour represents the highest or lowest level of expression respectively. (B) Fold expression levels of affected genes under HFD conditions in WT, *Tert*$^{-/-}$ and *Terc*$^{-/-}$ mouse livers. Results were normalized to WT samples. (C) Heat map of hepatic expression of fatty liver genes from *Tert*$^{-/-}$ and *Terc*$^{-/-}$ mouse livers under RD and HFD conditions. (D–E) Fold expression of affected genes. (F) Heat map of *Tert*$^{-/-}$ and *Terc*$^{-/-}$ mouse livers under RD conditions. (G) Fold expression of *Abca1* and *Insr* genes. Error bars represent SD. Statistical significance was determined by One-way ANOVA *$P < .05$; **$P < .002$. Data represent two mice/group from two independent experiments

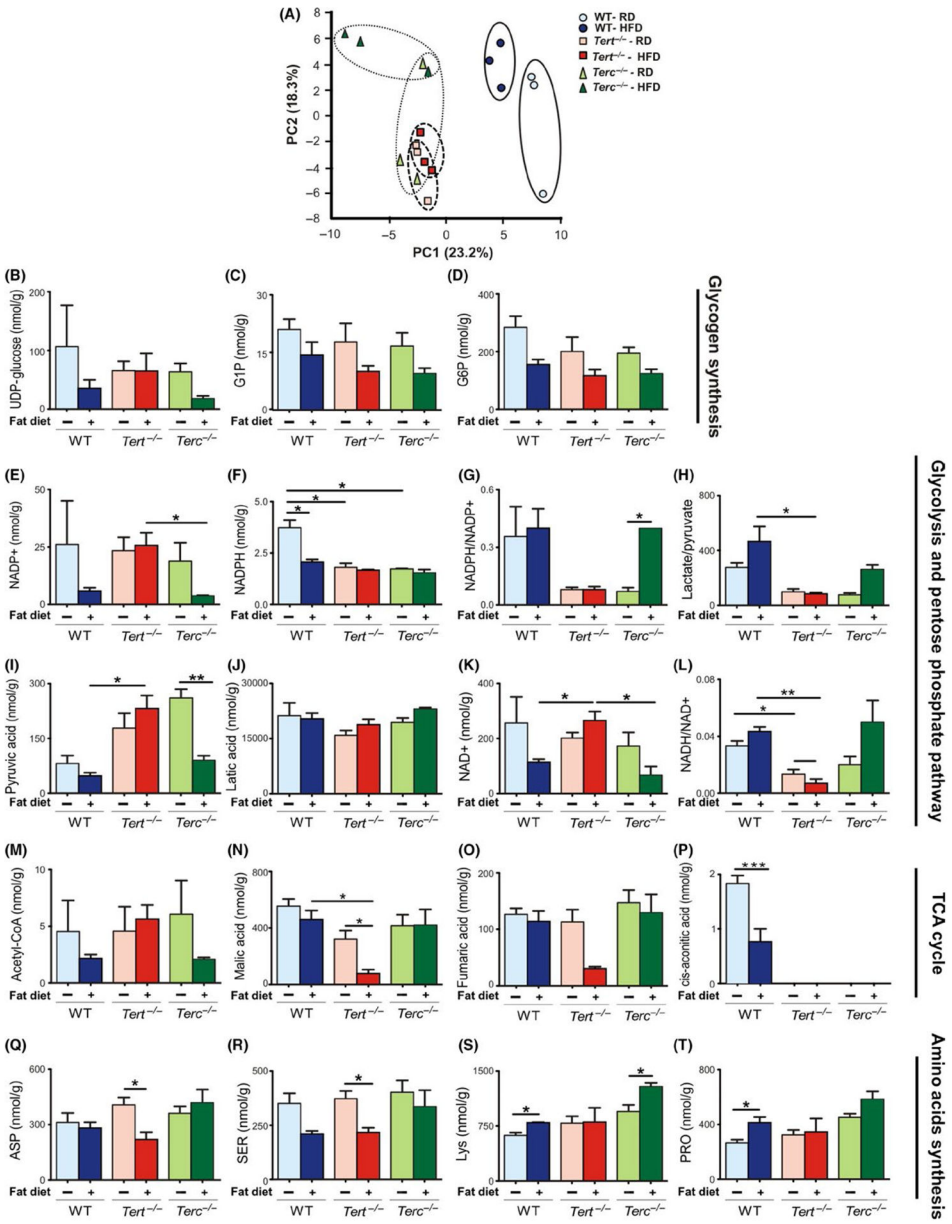

FIGURE 5.

Metabolic analysis in WT, *Tert*$^{-/-}$ and *Terc*$^{-/-}$ mouse livers. (A) PCA score plot showing the two first principal components for NMR spectra obtained on chloroform extracts of liver samples from mice under RD and HFD conditions. (B–D) Compounds related to glycogen synthesis. (E–L) Detection of compounds related to glycolysis and pentose phosphate pathway, and (M–P) compounds affecting the TCA cycle under HFD. (Q–T) Amino acid levels in WT, *Tert*$^{-/-}$ and *Terc*$^{-/-}$ mouse livers after HFD condition. Error bars represent SD. Statistical significance was determined by one-way ANOVA $*P < .05$; $**P < .001$; $***P < .0001$. Data represent three mice/group